Proceedings of the 10th World Congress on Momentum, Heat and Mass Transfer (MHMT 2025)
Barcelona, Spain - April 10 - 12, 2025
Paper No. ICMFHT 103
DOI: 10.11159/icmfht25.103

On the Recovery of the Exact Momentum Jump of highly Viscous Flows in Phase-Change Simulations with a One-Fluid Formulation

Jordi Poblador-Ibanez, Bendiks Jan Boersma
Delft University of Technology
Mekelweg 2, Delft, 2628 CD, The Netherlands
J.PobladorIbanez@tudelft.nl; B.J.Boersma@tudelft.nl

Abstract **-** The one-fluid formulation of the governing equations of fluid motion is an accepted methodology to solve two-phase flows. The discontinuity at the phase interface is regularized as a single fluid with varying properties and additional source terms are added, such as surface tension, to satisfy jump conditions. While such an approach is well-suited for non-evaporative flows, multiple inconsistencies arise in flows undergoing phase change due to the local volume dilatation at the interface, both in terms of analytical description and numerical discretization, that may affect the flow dynamics. That is, the numerical solution is more sensitive to the choice of formulation and discretization of the governing equations, as well as the interface capturing method, e.g., Volume-of-Fluid (VOF). Starting from the non-conservative one-fluid formulation of the momentum equation for incompressible flows, corrections to the momentum balance are implemented in the presence of phase change. The addition of two body forces in the context of the Continuum Surface Force model and the definition of two predictor-projection steps (pressure-velocity coupling) have been shown to recover the correct pressure jump in the limit of low viscosity while using standard discretization schemes in the one-fluid framework. However, issues remain with the regularization of the viscous term due to the discrete evaluation of the one-fluid velocity gradients, creating a momentum imbalance. Within a sharp VOF framework, various methods to correct the viscous term are analysed and discussed by considering a saturated vapor bubble growing in superheated liquid of a highly viscous fluid designed for numerical validation purposes.

Keywords**:** boiling flows, volume-of-fluid, one-fluid formulation, momentum balance, phase change

1. Introduction

The development of accurate multiphase flow solvers is a challenging pursuit, especially when significant phase change occurs such as in liquid fuel evaporation during injection [1], coolant boiling in heat exchangers [2] or hydrogen bubble formation in water electrolysis [3]. The one-fluid formulation of the Navier-Stokes equations where the two phases are treated as a single fluid whose properties are regularized across the resolved interface is widely used [4]-[6]. Moreover, this method ensures jump conditions are satisfied by including additional source terms localized at the interface, such as surface tension in the momentum equation [7]. Recently, Trujillo [8] has shown that, despite conservative and non-conservative forms of the governing equations are used interchangeably in the literature, their equivalency at the interface is only true in the limit of non-evaporative flows. For example, the non-conservative form of the one-fluid momentum equation is widely used in phase change simulations, e.g., see [6], perhaps due to the simplicity of directly extending existing codes. However, inconsistencies arise from the time derivative and convective terms when phase change occurs that cause a momentum imbalance at the interface. In contrast, a conservative formulation may recover the exact momentum jump. Note that beyond the analytical evaluation of the jump conditions from the governing equations, other errors may be introduced by the choice of numerical method, integration and discretization techniques.

Using a geometric Volume-of-Fluid (VOF) method to capture the interface due to its mass-conserving properties and sharp interface representation, [9] has shown that the addition of two body forces within the context of the Continuum Surface Force (CSF) model [7] and a careful rethinking of the pressure-velocity coupling algorithm are able to recover the exact momentum balance across the interface for fluids with low viscosity in a non-conservative formulation, resulting in a physical pressure jump. Thus, this one-fluid framework more suited for a sharp VOF approach can provide a consistent solution similar to Ghost Fluid Methods (GFM) [10]. Moreover, the momentum imbalance in the non-conservative framework is also evident in configurations where the impact of phase change is seemingly negligible, with the additional body forces and

algorithm steps resulting in a smoother temporal evolution of the pressure jump and slightly different flow dynamics (e.g., change in rise velocity of a vaporizing bubble).

Problems with the momentum imbalance in the one-fluid formulation resurface when the viscosity of the fluid is high due to the ill-defined discrete evaluation of the viscous term, i.e., the gradient of a velocity field that varies sharply across the interface. Independent of the choice between conservative and non-conservative formulation of the momentum equation, this issue also affects the flow dynamics, such as delaying the instability growth and bubble formation in film boiling [9]. In this paper, the numerical framework and momentum balance corrections described in [9] are summarized. Then, various approaches to attempt to obtain the correct momentum jump when viscosity dominates are explored and discussed within the possibilities of a VOF framework.

2. Governing Equations and Numerical Methods

This section briefly summarizes the main features of the flow solver described in [9] to study incompressible evaporating two-phase flows. For further details related to, e.g., the discretization of the various terms, the definition of a thin interfacial region Ω_Γ and its regularization, the time step evaluation or the validation of the solver, the reader is referred to [9] and the references therein. Note that the numerical framework is based on a Cartesian uniform grid with staggered velocity components.

2.1. Volume-of-Fluid Framework

A geometrical VOF based on the local reconstruction of the interface at each cell is used. The interface shape, orientation and cut volumes are obtained from a Piecewise Linear Interface Construction (PLIC) where the normal unit vector $\boldsymbol{n}_\Gamma$ (pointing from liquid to gas) and curvature κ (defined positive for convex liquid shape) are obtained, respectively, from the Mixed-Youngs-Center method and Height Function method [9]. Additionally, the calculations of geometric fluxes and κ are enhanced by a Piecewise Parabolic Interface Construction (PPIC) via the Interface Reconstruction Library [11]. If the PPIC reconstruction is ill-defined, the method defaults back to standard PLIC. Then, the interface is advected by solving Eq. (1) for the phase indicator X which includes an additional source term due to the mass transfer across phases. Here, $\mathrm{X} = 1$ in the liquid. The advection is performed by first shifting the interface plane along $\mathbf{n}_\Gamma$ to account for phase change [6] and, then, using a conservative split advection scheme with a divergence-free phase-wise velocity [5]. Note that the volume fraction is given by $C = \frac{1}{V_c}\int_{V_c} \mathrm{X} dV$, where V_c is the cell volume; $\dot{m}'$ is the mass flux per unit area ($\dot{m}' > 0$ for vaporization) and δ_Γ is a Dirac delta function only active at the interface; and the phase-wise velocity and density in Eq. (1) are representative of the liquid (L) or gas (G) phase depending on whether the flow is laden with droplets or bubbles [5].

$$\frac{\partial \mathrm{X}}{\partial t} + \nabla \cdot (\mathrm{X}\mathbf{u}_L) - \mathrm{X}(\nabla \cdot \mathbf{u}_L) = -\frac{\dot{m}'}{\rho_L}\delta_\Gamma \tag{1}$$

2.2. Mass and Momentum Transport

The non-conservative one-fluid formulation of the Navier-Stokes equations for incompressible two-phase flows undergoing phase change are given by the continuity equation, Eq. (2), and the momentum equation, Eq. (3),

$$\nabla \cdot \mathbf{u} = \dot{m}'\left(\frac{1}{\rho_G} - \frac{1}{\rho_L}\right)\delta_\Gamma \tag{2}$$

$$\rho\left(\frac{\partial \mathbf{u}}{\partial t} + \mathbf{u} \cdot \nabla \mathbf{u}\right) = -\nabla p + \nabla \cdot \mathbf{T} + \rho \mathbf{g} + \mathbf{f}_\sigma + \mathbf{f}_{\dot{m}'} + \mathbf{f}_{NC} \tag{3}$$

where $\mathbf{u}$ is the one-fluid velocity, p the pressure, $\mathbf{g}$ the gravity acceleration, $\mathbf{T} = \mu[\nabla \mathbf{u} + \nabla \mathbf{u}^T]$ the viscous stress tensor, ρ and μ the volume-averaged density and viscosity, e.g., $\rho = \rho_L C + \rho_G(1 - C)$, σ the surface tension coefficient, and $\mathbf{f}_\sigma = -\sigma\kappa\mathbf{n}_\Gamma\delta_\Gamma$. The terms $\mathbf{f}_{\dot{m}'} = -(\dot{m}')^2(\rho_G^{-1} - \rho_L^{-1})\mathbf{n}_\Gamma\delta_\Gamma$ and $\mathbf{f}_{NC} = \rho\dot{m}'(\rho_G^{-1} - \rho_L^{-1})(\mathbf{u} \cdot \mathbf{n}_\Gamma)\mathbf{n}_\Gamma\delta_\Gamma$ are additional body forces discretized in the context of the CSF model to recover the exact momentum balance across the interface in the limit of low

viscosity flows [9]. This momentum balance normal to the interface is given in terms of a pressure jump, i.e., Eq. (4). Tangent to the interface, the velocity and shear stress are continuous.

$$p_L - p_G = \sigma\kappa + (\dot{m}')^2\left(\frac{1}{\rho_G} - \frac{1}{\rho_L}\right) + ([\mathbf{T}_L - \mathbf{T}_G]\cdot\mathbf{n}_\Gamma)\cdot\mathbf{n}_\Gamma, \tag{4}$$

The flow solver is based on the predictor-projection approach by Chorin [12], modified with two predictor-projection steps, coupled to the extension of the split pressure gradient method by Cifani [13]. Altogether, a direct pressure solver can be used, which is computationally more efficient than other iterative methods [4]. As shown in [9], the addition of a first predictor-projection step is necessary to address the impact on the momentum balance of the time derivative in Eq. (3). This step evaluates a predicted velocity $\mathbf{u}^* = \mathbf{u}^n - \nabla\psi$ resulting from the shift in the Stefan flow across the interface from time t^n to t^{n+1} using a velocity potential ψ. In other words, solving the Poisson equation, Eq. (5), with the direct solver. Then, the standard predictor-projection approach, e.g., [13], is used to evaluate a predicted velocity $\mathbf{u}^{**}$ from $\mathbf{u}^*$ in Eq. (3) and to obtain $\mathbf{u}^{n+1}$ and p^{n+1}, where $\mathbf{f}_{NC}$ takes care of cancelling the ill-defined one-fluid convective term at the interface while $\mathbf{f}_{\dot{m}'}$ adds the correct momentum jump caused by the change of phase [9]. In summary, the corrections to the momentum balance are defined by the addition of a "pre-conditioner" predictor-projection step and the two forces $\mathbf{f}_{\dot{m}'}$ and $\mathbf{f}_{NC}$.

$$\nabla^2\psi = \nabla\cdot\mathbf{u}^n - \nabla\cdot\mathbf{u}^* = \dot{m}'\left(\frac{1}{\rho_G} - \frac{1}{\rho_L}\right)\delta_\Gamma\Big|^n - \dot{m}'\left(\frac{1}{\rho_G} - \frac{1}{\rho_L}\right)\delta_\Gamma\Big|^{n+1} \tag{5}$$

The preliminary shift of the Stefan flow follows the practice of advecting the interface before solving the Navier-Stokes equations, which results in the use of volume-averaged fluid properties at t^{n+1} [4]. Thus, variables tightly related to the interface location, such as the Stefan flow, must correspond to t^{n+1}. In practice, the use of $\mathbf{u}^*$ instead of $\mathbf{u}^n$ in the evaluation of Eq. (3) has a minimal impact in the single-phase region, but becomes necessary in Ω_Γ where $\mathbf{u}$ varies sharply. However, the approach embeds the assumption that the interface regression with respect to the fluid is a quasi-steady process; thus, any information of the change in Stefan flow from t^n to t^{n+1} is removed from the obtained pressure field everywhere.

2.3. Energy Transport

The energy equation is given in its non-conservative form by Eq. (6), where T is the temperature, c_p the isobaric specific heat and k the thermal conductivity. Following previous literature, e.g., [14], the energy equation is solved in a phase-wise manner. Here, each phase is treated separately with the interface as a deforming boundary embedded in the discretization of Eq. (6). Then, the interface thermodynamic state is implicitly accounted for and no additional source terms are needed. For the purpose of this work, the interface remains at saturation conditions given the system pressure; thus, its temperature is given by T_{sat}. The mass flux across the interface is evaluated from Eq. (7), where h_{LV} is the latent heat of vaporization. The temperature gradients normal to the interface are obtained with the normal probe technique described in [9].

$$\rho c_p\left(\frac{\partial T}{\partial t} + \mathbf{u}\cdot\nabla T\right) = \nabla\cdot(k\nabla T) \tag{6}$$

$$\dot{m}' = \frac{[k_G\nabla T_G - k_L\nabla T_L]\cdot\mathbf{n}_\Gamma}{h_{LV}} \tag{7}$$

3. Results

3.1. Momentum Balance Recovery in Low Viscosity

A couple of validation tests with an imposed $\dot{m}'$ for which an analytical solution can be obtained (see [9]) are meant to highlight the momentum balance corrections introduced in Section 2.2 by looking at the improvement in the calculation of the pressure field. For both tests, $\dot{m}' = 10$ kg/(m^{2}s) and the properties of each phase are $\rho_L = 500$ kg/m^3, $\mu_L = 50$ μPa·s, $\rho_G = 100$ kg/m^3 and $\mu_G = 25$ μPa·s. In [9], the performance of the flow solver is further addressed by considering a wide range of density and viscosity ratios, different surface tension coefficients, dynamic configurations, and the coupling with the energy equation. The first test (shown in Fig. 1a) analyses a liquid pool sitting on a wall located at $x = 0$ with the interface

initially at $x_0 = 25$ mm. Interface deformation is neglected, thus a one-dimensional evolution is expected. In contrast, the second test looks at the evaporation of a static droplet (three-dimensional) of an initial radius $r_0 = 12.5$ mm and a surface tension coefficient $\sigma = 1$ mN/m. In both cases, a reference pressure of 0 Pa is imposed in the gaseous domain boundary, which is set sufficiently far away from the liquid-gas interface, and a mesh size of 0.390625 mm is used.

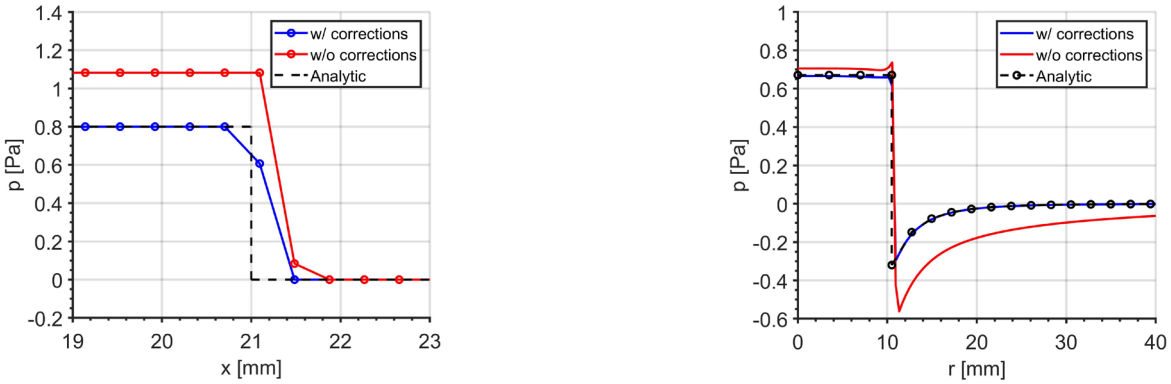

(a) One-dimensional liquid surface (b) Static evaporating droplet

Fig. 1: Validation tests of the momentum balance corrections in the limit of low viscosity in terms of the pressure field solution. (a) one-dimensional evaporating liquid surface at $t = 0.2$ s; (b) static droplet evaporation at $t = 0.1$ s.

As shown in Fig. 1, the addition of the corrective body forces and predictor-projection step shifting the Stefan flow recover both the correct pressure jump across the interface and the analytical solution. Note that for the droplet, the analytical solution is derived under the quasi-steady state assumption of the interface regression discussed in Section 2.2 [9]. In particular, the non-corrected formulation results in a higher liquid pressure in the one-dimensional case, while a smaller pressure is obtained in the gas in the droplet case. Note that this is partially a result of the interaction between an ill-defined momentum balance and the boundary conditions of each problem, as well as the quasi-steady assumption. Noteworthy, the corrections only affect the consistency of the pressure field since the velocity is imposed via Eq. (2). While this seems to not be problematic when analysing static configurations, such as the evaporation of a droplet or the growth of a bubble, the prediction of an ill-defined pressure balance does affect dynamic cases [9].

3.2. Discretization of the Viscous Term

For highly viscous flows, the regularization of the viscous term in Eq. (3) fails. This has no direct relation with the manner in which μ is averaged (i.e., arithmetic vs. harmonic mean) in the vaporizing fluid, but rather is a result of the discrete evaluation of $\nabla \mathbf{u}$ when the velocity varies sharply across Ω_Γ. As a result, a momentum imbalance is again introduced, usually resulting in a pressure spike across the interface, that can affect the dynamical evolution of the two-phase flow. This direct evaluation of $\mathbf{T}$ is referred to as one-fluid approach in what follows. In this work, three other approaches to improve the discretization of $\mathbf{T}$ within the one-fluid framework are proposed and analysed. For all of them, the term is treated phase-wise and standard second-order differentiation in the staggered mesh is used. That is, no averaging is performed for μ and a constant value μ_L or μ_G is selected depending on the predominant phase in the cell, e.g., μ_L if $C \geq 0.5$ in the staggered cell used for the discretization of Eq. (3). The same criterion is used to select a phase-wise velocity, determined as follows.

The first approach (I) consists of performing a constant extrapolation normal to the interface of the velocity components in each cell, effectively obtaining two phase-wise velocities $\mathbf{u}_G$ and $\mathbf{u}_L$. An efficient Fast Marching Method (FMM) [15] can be integrated in the VOF framework for this purpose [9]. While the use of $\mathbf{u}_G$ and $\mathbf{u}_L$ will improve the calculation of the velocity gradients and mitigate the pressure spike in the viscous term, $\mathbf{u}_G$ and $\mathbf{u}_L$ are not divergence-free by construction.

The second approach (II) consists in constructing $\mathbf{u}_G$ and $\mathbf{u}_L$ such that $\nabla \cdot \mathbf{u}_G = 0$ and $\nabla \cdot \mathbf{u}_L = 0$. Different methods can be used to achieve this. In particular, one of the phase-wise velocities satisfying the divergence-free condition is already obtained during the VOF advection step, depending on the two-phase configuration, as discussed in Section 2.1. The other may be obtained by solving a Poisson equation in a narrow band around the interface, such as in [6], which can be certainly expensive in some scenarios and defeats the purpose of working with direct solvers in the predictor-projection steps.

The third and last approach (III) takes a different route. A constant extrapolation normal to the interface of the velocity gradient is performed with the FMM technique, obtaining the phase-wise gradients $\nabla\mathbf{u}_G$ and $\nabla\mathbf{u}_L$. These replace the discrete gradients in $\mathbf{T}$ if, when calculated with $\mathbf{u}$, velocity values across Ω_Γ are used. That is, where $\dot{m}'(\rho_G^{-1} - \rho_L^{-1})\delta_\Gamma \neq 0$. Since a constant extrapolation of $\nabla\mathbf{u}$ along $\mathbf{n}_\Gamma$ results in, e.g., $\nabla^2\mathbf{u}_G \approx 0$ along $\mathbf{n}_\Gamma$, a pressure jump across Ω_Γ due to the viscous stresses is not expected to be obtained numerically. In other words, the viscous term is effectively cancelled in Ω_Γ, similar to how $\mathbf{f}_{NC}$ cancels the convective term. As discussed in [9], this is not problematic since $\mathbf{u}^{n+1}$ in Ω_Γ is entirely driven by Eq. (2), but requires the addition of a body force to impose the physical pressure gradient or jump across the interface, such as $\mathbf{f}_{\dot{m}'}$. For the viscous stress jump, a new regularized force $\mathbf{f}_\mu = [\mathbf{T}_G - \mathbf{T}_L] \cdot \mathbf{n}_\Gamma \delta_\Gamma$ is added to the right-hand side of Eq. (3) and treated similar to the other forces in the flow solver [9]. It is calculated based on the actual viscous stress jump in the momentum balance (see Eq. (4)), with $\mathbf{T}_G$ and $\mathbf{T}_L$ using phase-wise viscosities and velocity gradients, i.e., those extrapolated with the FMM. While $\mathbf{f}_{\dot{m}'}$ and $\mathbf{f}_{NC}$ are purely built upon a one-fluid formulation, the phase-wise discretization of the viscous term and addition of $\mathbf{f}_\mu$ are related more closely to the GFM [10].

3.3. Static Bubble Growth in Superheated Liquid

The proposed corrections to the viscous term in the momentum equation are tested in a configuration involving a static saturated vapor bubble growing in superheated liquid. Analytical solutions under spherical symmetry for the bubble radius, Eq. (8), and temperature evolution in the liquid, Eq. (9), are given by Scriven [16], with β being the growth constant calculated with Eq. (10), T_∞ the superheated temperature, and $\alpha = h_{LV} + (c_{p,L} - c_{p,G})(T_\infty - T_{sat})$. Further, an approximate analytical solution for the radial velocity is given by Eq. (11), which is obtained directly from the continuity equation by decoupling its calculation from the pressure. Then, by substitution into the radial momentum equation under the assumptions that $p_{r\to\infty} = 0$ and that the interface regression is a quasi-steady process, an equation for the pressure radial distribution, Eq. (12), is obtained. In Eqs. (11) and (12), $U_L = \dot{m}'(\rho_G^{-1} - \rho_L^{-1})$ as a result of the velocity jump across the interface.

$$R(t) = 2\beta\sqrt{\frac{k_L}{c_{p,L}\rho_L}t} \tag{8}$$

$$T(r,t) = T_\infty - 2\beta^2\left(\frac{\rho_G\alpha}{\rho_L c_{p,L}}\right)\int_{1-R(t)/r}^{1}\exp\left[-\beta^2\left((1-\xi)^{-2} - 2\left(1-\frac{\rho_G}{\rho_L}\right)\xi - 1\right)\right]d\xi \tag{9}$$

$$\frac{\rho_L c_{p,L}(T_\infty - T_{sat})}{\rho_G\alpha} = 2\beta^2\int_0^1\exp\left[-\beta^2\left((1-\xi)^{-2} - 2\left(1-\frac{\rho_G}{\rho_L}\right)\xi - 1\right)\right]d\xi \tag{10}$$

$$u_r(r,t) = \begin{cases} 0 & \text{if } r < R(t) \\ U_L(R(t)/r)^2 & \text{if } r \geq R(t) \end{cases} \tag{11}$$

$$p(r,t) = \begin{cases} -\frac{1}{2}\rho_L U_L^2 - \sigma\kappa - (\dot{m}')^2\left(\frac{1}{\rho_G} - \frac{1}{\rho_L}\right) + 4\frac{\mu_L}{R(t)}U_L & \text{if } r < R(t) \\ -\frac{1}{2}\rho_L U_L^2\left(\frac{R(t)}{r}\right)^4 & \text{if } r \geq R(t) \end{cases} \tag{12}$$

A specific set of fluid properties used in [6] or [14] based on a "test" fluid for validation purposes are shown to be problematic for the momentum balance due to the high fluid viscosity despite not affecting the overall growth of the bubble and evolution of the temperature field due to the static configuration [9]; thus, it highlights the intrinsic issues in the discretization of the viscous term. The properties of the test fluid are $\rho_L = 2.5$ kg/m^3, $\mu_L = 7$ mPa·s, $k_L = 70$ mW/(m·K), $c_{p,L} = 2.5$ J/(kgK), $\rho_G = 0.25$ kg/m^3, $\mu_G = 0.7$ mPa·s, $k_G = 7$ mW/(m·K), $c_{p,G} = 1$ J/(kgK), $\sigma = 1$ mN/m, $T_{sat} = 1$ K and $h_{LV} = 100$ J/kg. For this specific problem, $T_\infty = 3$ K. The bubble size and temperature distribution are initialized with the

analytical solution at $t = 0.5$ s (i.e., $R_0 \approx 0.117$ m). The domain is large enough to limit the influence of its boundaries on the bubble growth, which are defined as open boundaries. Three mesh sizes are considered, defined by mesh V1 ($\Delta x = 1/64$ m), mesh V2 ($\Delta x = 1/128$ m) and mesh V3 ($\Delta x = 1/192$ m). More details on the computational setup can be found in [9].

The validation against Scriven's solution is performed up to $t = 2$ s in [9]; thus, it is not included here since the scope of the paper is addressing the discretization of the viscous term. Fig. 2a shows the evolution of the bubble radius (obtained from the volume of the bubble) up to $t = 0.6$ s with approach III, which converges with mesh refinement. One undesired effect of the different viscous term treatments is shown in Fig. 2b, which compares the radius evolution among all discretization approaches, including the one-fluid approach, with the finest mesh V3. With approach II, the bubble does not evolve spherically and the estimated radius deviates significantly from the analytical solution. In contrast, the other methods behave well, with approach III reproducing the results from the one-fluid approach the closest. Fig. 2c shows the convergence to the analytical solution of the temperature radial profile at $t = 0.6$ s for approach III, extracted along the z direction. Here, no major differences are appreciated between different methods.

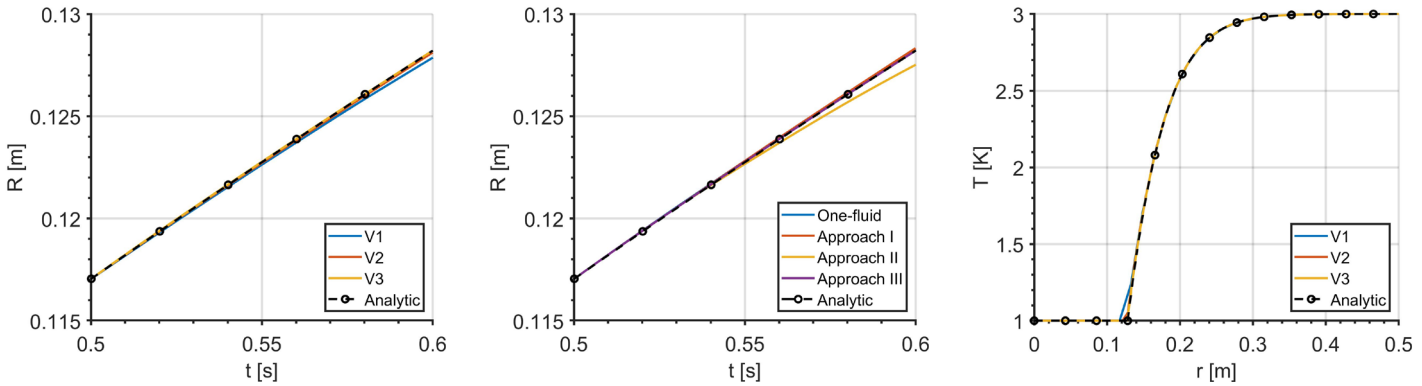

(a) Radius growth with approach III (b) Radius growth with mesh V3 (c) Temperature at 0.6 s with approach III

Fig. 2: Validation of static vapor bubble growth in superheated liquid against Scriven's analytical solution [16]. (a) mesh convergence of radius growth with approach III; (b) radius growth obtained with mesh V3 and different modelling approaches for the viscous term; (c) mesh convergence of temperature profile at $t = 0.6$ s with approach III, extracted along the z direction.

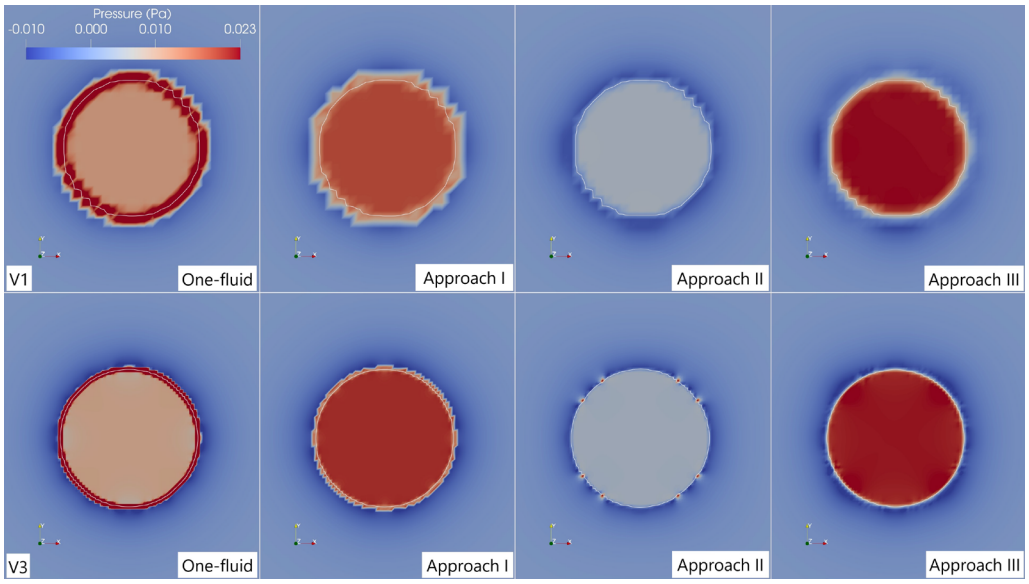

Fig. 3: Pressure field inside and around the vapor bubble at $t = 0.6$ s on an xy plane across the bubble. The various approaches to discretize the viscous term are shown with mesh V1 (top) and mesh V3 (bottom).

The impact of the discretization of $\mathbf{T}$ on the pressure field is visualized in Figs. 3 and 4 for $t = 0.6$ s. Fig. 3 shows contours of the pressure field on an xy plane across the bubble. Immediately, one observes the pressure spike across the interface occurring with the one-fluid formulation due to the ill-defined $\nabla\mathbf{u}$ when calculating $\mathbf{T}$. In contrast, approaches I, II and III eliminate the jump and recover a different pressure inside the bubble. As shown in Fig. 4a, the pressure spike goes well beyond the figure bounds, i.e., $p_{max} \approx 0.13$ Pa, and a smaller pressure inside the bubble than the analytical solution is obtained. For reference, the contributions to the pressure jump $\Delta p = p_G - p_L$ at $t = 0.6$ s are $-\sigma\kappa = 0.015599$ Pa, $-(\dot{m}')^2(\rho_G^{-1} - \rho_L^{-1}) = -0.002719$ Pa and $4\mu_L U_L/R = 0.021606$ Pa, with $R = 0.12821$ m and $\dot{m}' = 0.027481$ kg/(m^{2}s). When comparing the phase-wise approaches, approach II also predicts a smaller pressure inside the bubble but approach I and III approximate the analytical solution. Note that approach I still presents some oscillation across Ω_Γ while III behaves more consistently with a smoother jump distribution that converges to the analytical solution (see Fig. 4c). That is, III does seek to eliminate the numerical influence of $\mathbf{T}$ in Ω_Γ to replace it with $\mathbf{f}_\mu$. From Fig. 3, the smoother pressure distribution obtained with approach III, despite some evidence of spurious oscillations, is highlighted when compared to the sharpness of approaches I and II. In particular, II displays sporadic pressure spikes due to limits in the divergence-free extrapolation of $\mathbf{u}_G$ and $\mathbf{u}_L$ with a Poisson-type equation, e.g., localized convergence issues, that could also be linked to the deteriorating shape implied by the radius growth profile in Fig. 2b.

Notably, approach I may reach a similar effect as III due to the combination of the specific numerical discretization (central differencing) and problem configuration (static bubble). Specifically, it approximates $\mathbf{u}_G \approx 0$, resulting in $\nabla^2\mathbf{u}_G \approx 0$, and obtains $\nabla^2\mathbf{u}_L$ from a finite difference scheme that differentiates between two velocity gradients across the interface where one is nearly zero due to the constant velocity extrapolation and the other approximates the correct phase-wise gradient, resulting in a pressure jump similar to that introduced by $\mathbf{f}_\mu$. Similarly, the particular configuration results in approach II almost cancelling the influence of $\mathbf{T}$ across Ω_Γ (thus the reduced pressure jump) and the addition of $\mathbf{f}_\mu$ could yield a similar result as approach III. That is, by realizing that II may be providing $\mathbf{u}_G \approx 0$ and $\mathbf{u}_L$ approximately linear along $\mathbf{n}_\Gamma$, so $\nabla^2\mathbf{u}_G \approx 0$ and $\nabla^2\mathbf{u}_L \approx 0$ along the normal direction. Regardless, the consistency of approach III is preferred.

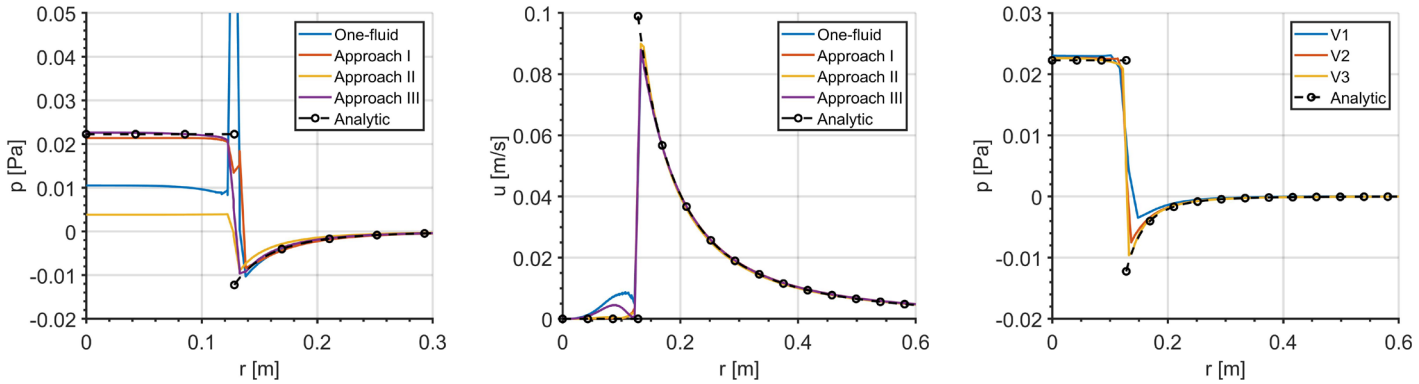

(a) Pressure field with mesh V3 (b) Radial velocity with mesh V3 (c) Pressure field with approach III

Fig. 4: Radial profiles of pressure and velocity of the static vaporizing bubble extracted along the z direction at $t = 0.6$ s. (a) pressure obtained with mesh V3 and different modelling approaches for the viscous term; (b) velocity obtained with mesh V3 and different modelling approaches for the viscous term; (c) mesh convergence of the pressure with approach III.

Lastly, Fig. 4b plots the radial velocity distribution at $t = 0.6$ s. While all methods perform well in reproducing the analytical solution in the liquid phase, some non-zero velocity is observed in the vapor due to the presence of spurious currents in the VOF framework. The standard one-fluid discretization behaves the worst, while approach III mitigates the issue. However, approaches I and II provide a more consistent velocity inside the bubble despite the drawbacks in correcting the momentum balance and providing a consistent pressure field. Note that the presence of spurious currents is not seen to harm the long-term agreement with Scriven's analytical solution [9].

4. Conclusion

This paper has extended a momentum-consistent one-fluid formulation for low-viscosity evaporating flows recently developed using a non-conservative momentum formulation together with a sharp geometric VOF [9] to flows with high

viscosity. Regardless of the conservative or non-conservative formulation, the discretization of the viscous term in the one-fluid context can introduce momentum imbalances that result in a non-physical pressure jump across the interface. Although its impact in static configurations is limited, such imbalances may be detrimental in more dynamic setups, e.g., instability timescales in boiling simulations. That is, the evolution of the liquid-gas interface strongly depends on the pressure jump across it. Within the context of the CSF model, three different approaches have been tested to discretize the viscous term in a phase-wise manner. A methodology based on the constant extrapolation normal to the interface of the velocity gradient and the addition of a body force to replicate the momentum jump induced by the viscous stresses is shown to provide a consistent numerical behaviour and recovers the exact pressure jump. Closely related to the GFM, such approach aims at the cancellation of the influence of the viscous term in the interfacial region and replaces it by a body force that generates a controlled pressure jump across the interface.

Acknowledgements

This publication is part of the Small Compute project *Development of High-Fidelity Multiphase Solver for Boiling Flows* of the research programme *Computing Time on National Computer Facilities* which is (partly) financed by the Dutch Research Council (NWO). This work used the Dutch national e-infrastructure with the support of the SURF Cooperative using grant no. EINF-9679. The authors also acknowledge the use of computational resources of DelftBlue supercomputer, provided by Delft High Performance Computing Centre (https://www.tudelft.nl/dhpc).

References

[1] X. Gao, J. Chen, Y. Qiu, Y. Ding, and J. Xie, "Effect of phase change on jet atomization: a Direct Numerical Simulation study," *J. Fluid Mech.*, vol. 935, pp. A16, 2022.
[2] E. M. J. Komen, A. Mathur, F. Roelofs, E. Merzari, and I. Tiselj, "Status, perspectives, and added value of high fidelity simulations for safety and design," *Nucl. Eng. Des.*, vol. 491, pp. 112082, 2023.
[3] A. Taqieddin, Y. Liu, A. N. Alshawabkeh, and M. R. Allshouse, "Computational Modeling of Bubbles Growth Using the Coupled Level Set – Volume of Fluid Method," *Fluids*, vol. 5, no. 3, pp. 120, 2020.
[4] M. S. Dodd and A. Ferrante, "A fast pressure-correction method for incompressible two-fluid flows," *J. Comput. Phys.*, vol. 273, pp. 416-434, 2014.
[5] N. Scapin, P. Costa, and L. Brandt, "A Volume-of-Fluid method for interface-resolved simulations of phase-changing two-fluid flows," *J. Comput. Phys.*, vol. 407, pp. 109251, 2020.
[6] L. Malan, A. Malan, S. Zaleski, and P. Rousseau, "A geometric VOF method for interface resolved phase change and conservative thermal energy advection," *J. Comput. Phys.*, vol. 426, pp. 109920, 2021.
[7] J. Brackbill, D. Kothe, and C. Zemach, "A continuum method for modeling surface tension," *J. Comput. Phys.*, vol. 100, no. 2, pp. 335-354, 1992.
[8] M. F. Trujillo, "Reexamining the one-fluid formulation for two-phase flows," *Int. J. Multiph. Flow*, vol. 141, pp. 103672, 2021.
[9] J. Poblador-Ibanez, N. Valle, and B. J. Boersma, "A Momentum Balance Correction to the Non-Conservative One-Fluid Formulation in Boiling Flows using Volume-of-Fluid," *J. Comput. Phys.*, vol. 524, pp. 113704, 2025.
[10] L. Anumolu and M. F. Trujillo, "Gradient augmented Level Set method for phase change simulations," *J. Comput. Phys.*, vol. 353, pp. 377-406, 2018.
[11] F. Evrard, R. Chiodi, A. Han, B. van Wachem, and O. Desjardins, "First moments of a polyhedron clipped by a paraboloid," *SIAM J. Sci. Comput.*, vol. 45, no. 5, pp. A2250-A2274, 2023.
[12] A. J. Chorin, "Numerical solution of the Navier-Stokes equations," *Math. Comput.*, vol. 22, no. 104, pp.745-762, 1968.
[13] P. Cifani, "Analysis of a constant-coefficient pressure equation method for fast computations of two-phase flows at high density ratios," *J. Comput. Phys.*, vol. 398, pp. 108904, 2019.
[14] B. Boyd and Y. Ling, "A consistent Volume-of-Fluid approach for direct numerical simulation of the aerodynamic breakup of a vaporizing drop," *Comput. Fluids*, vol. 254, pp. 105807, 2023.
[15] J. O. McCaslin, E. Courtine, O. Desjardins, "A fast marching approach to multidimensional extrapolation," *J. Comput. Phys.*, vol. 274, pp. 393-412, 2014.
[16] L. Scriven, "On the dynamics of phase growth," *Chem. Eng. Sci.*, vol. 10, no. 1, pp. 1-13, 1959.